Generalized diffractive optical elements with asymmetric harmonic response and phase control

Jorge Albero,[1] Jeffrey A. Davis,[2] Don M. Cottrell,[2] Charles E. Granger,[2] Kyle R. McCormick,[2] and Ignacio Moreno[1,*]

[1]Departamento de Ciencia de Materiales, Óptica y Tecnología Electrónica, Universidad Miguel Hernández, Elche 03202, Spain

[2]Department of Physics, San Diego State University, San Diego, California 92182-1233, USA

*Corresponding author: i.moreno@umh.es

Received 11 January 2013; revised 25 April 2013; accepted 25 April 2013; posted 26 April 2013 (Doc. ID 183030); published 20 May 2013

We report a method to generate phase-only diffractive beam splitters allowing asymmetry of the target diffracted orders, as well as providing a tailored phase difference between the diffracted orders. We apply a well-established design method that requires the determination of a set of numerical parameters, and avoids the use of image iterative algorithms. As a result, a phase lookup table is determined that can be used for any situation where a first-order (blazed) diffractive element is modified to produce higher orders with desired intensity and/or phase relation. As examples, we demonstrate the phase difference control on triplicators, as well as on other generalized diffractive elements like bifocal Fresnel lenses and phase masks for the generation of vortex beams. Results are experimentally demonstrated by encoding the calculated phase pattern onto parallel-aligned liquid crystal spatial light modulators.

OCIS codes: (050.1950) Diffraction gratings; (050.1970) Diffractive optics.
http://dx.doi.org/10.1364/AO.52.003637

1. Introduction

The potential for diffractive optical elements (DOEs) depends to a great extent on their optical efficiency, which is defined as the fraction of the total energy diffracted into a desired order. Continuous blazed phase-only gratings have the greatest efficiency because all of the energy is diffracted into a single first-order [1], but they are difficult to fabricate. In more common binary amplitude or binary phase devices, numerous diffracted orders are produced with symmetric intensities [2]. These gratings are fabricated by taking the original blazed grating and dividing each period into two segments that are encoded with different binary amplitudes or binary phases (typically 0 or π rad). Dammann gratings are of interest because they produce equal intensities in a given number of orders [3]. These Dammann gratings are fabricated, again by subdividing each period into regions with phase values of 0 or π rad. The transition points are carefully controlled to achieve the desired number of orders and optical efficiency [4]. Other binarization schemes follow fractal structures [5].

In both cases of simple binary or Dammann gratings, the ideas have been applied to more general functions including lenses [6], vortex sensing diffraction gratings [7], and filters for optical pattern recognition [8]. One simply takes the continuous blazed phase profile for these other optical elements and applies the appropriate binary phase structure

1559-128X/13/153637-08$15.00/0

to achieve a number of higher orders of the original function. For example, with a lens structure having a focal length f, the Dammann or binary process leads to a series of lens functions having focal lengths of f/n (n denoting the harmonic order) and intensities related to the Fourier coefficients of the binary process. The desired optical elements for each of these cases can be easily generated by taking the original continuous blazed phase mask and applying a look-up table to map the phases accordingly. Excellent experimental results have been obtained for many of the examples mentioned above. It is interesting to note that, in each of these cases, one could apply iterative computational approaches to achieve similar results [9–11]. However each case would require a separate iterative process.

In order to increase the optical efficiency of these Dammann gratings, Prongué *et al.* proposed a theoretical approach of optimal beam splitting [12]. The field of fan-out arrays was extensively developed in the late 80 s, and a good review of these early works can be found in [13], which includes both binary and continuous phase profiles. More recently, Romero and Dickey further extended [14,15], and provided a general framework for the design of optimal fan-out phase elements. This theory extends previous studies devoted to optimal triplicators [16], and provides an analytical optimal solution of the problem of designing a diffraction grating with a set of target diffraction orders. The calculation involves optimization of two numerical variables for each target order. In other words, one maximizes a single function that generates a periodic diffraction grating with continuous phase modulation levels. The method by Dickey and Romero is a general theory, in the sense that it can be used to design gratings with arbitrary target orders, as well as to control their relative intensity and phase. However, most of their designs are devoted to obtaining equi-intense light spots with spatial symmetry with respect to the optical axis. Furthermore, their practical implementation has been restricted only to these cases, which were demonstrated in [17,18], mainly due to the difficulty of fabricating these continuous phase-only profiles. As in the case of the binary or Dammann gratings, one could obtain similar results using general iterative algorithms that apply to the complete phase mask, such as inverse Fourier transform, or simulated annealing algorithms, as mentioned before.

In recent work, we extended the optimal theory for phase-only optimal beam splitting [19,20] to more general applications in several ways. First, we showed that the experimental realization of these complicated phase-only phase profiles could be realized using programmable liquid crystal spatial light modulators (LC-SLMs) [19]. The relatively high resolution achievable with modern devices (with pixel sizes in the range of tens of microns) has turned SLMs into a reliable choice for diffractive optics tasks. In addition, we found that the optimized grating could be easily computed using the SOLVER routine found in Microsoft Excel as discussed below. Finally and most importantly, we were able to implement this phase profile onto arbitrary phase-only gratings, similar to the approach with Dammann grating phase profiles shown in [7]. Moreover, working with a single equation is advantageous since the profile could be directly applied to other generalized DOEs. One simply applies a phase transformation using a look-up table to convert the initial phase profile to the new desired design. An initial demonstration of this combination was used to control the relative intensities of the diffracted beams in [20], where it was applied to design vortex generating/sensing gratings.

However, the potential of the optimal method has not been fully exploited. Two aspects not yet fully developed are the design of asymmetric gratings, and the control of the relative phase among the different target diffraction orders. In some cases, gratings that produce nonsymmetric intensities in the various diffracted orders are of interest. For example, Davis *et al.* used gratings where the diffraction was divided mainly between the zeroth and first-orders to impose amplitude information onto phase-only structures [21]. This 0th–1st grating duplicator was also studied in [22] with a four-step computer-generated hologram, with an overall efficiency $\eta = 0.766$. Efficiencies of 100% were obtained when reproducing this duplicator, but using waveplate gratings where polarization-control adds an additional degree of freedom [23]. A similar polarization approach was used to generate asymmetric triplicator with target orders 0th, 1st, and 2nd [24].

The control of the relative phase between the diffracted beams is also of interest, mainly for applications in interferometry or for phase visualization. For instance, a phase bias can be added to the zero-order to produce destructive interference in order to eliminate it, as demonstrated in [25]. Another example of application was reported in [26], where the interference of the 0th–1st diffraction orders was proposed to visualize the phase pattern of encoded helical Ince–Gaussian beams. This procedure was then extended to completely remove the contribution from the other orders in [27].

In this paper, we apply the phase-only based optical beam splitting theory of Romero and Dickey [14,15] to account for both, asymmetry of the target orders and phase control. First we show gratings with asymmetric dispositions of the various diffracted orders. These phase gratings with asymmetric output can be extended to other DOEs, such as diffractive lenses and vortex-producing lenses, where asymmetry can be an added value. For instance, a grating with asymmetric all-positive orders, when encoded onto a diffractive lens, generates a set of converging harmonic lenses. On the contrary, regular binary lenses, with positive and negative harmonic orders, generate both converging and diverging beams. Second, we demonstrate control over the phase of the diffracted orders. This last feature is

demonstrated with diffractive lenses, as well as with phase patterns for the generation of vortex beams.

The paper is organized as follows. In Section 2, a brief description of the theory of phase-only grating beam splitting is given, with special focus on our approach for the design of the gratings. Section 3 presents the experiments as well as a discussion, first on beam splitter gratings with asymmetric output and second on phase control of the diffracted beams. Two applications are discussed in Section 4, devoted to the generation of a bifocal diffractive lens, with relative phase control of the two converging beams, and the generation of vortex beams, also with control of their relative interference. Experimental results that verify the theoretical designs are obtained using two different setups that employ parallel-aligned LC-SLMs. Finally, conclusions are given in Section 5.

2. Theory of Optimal Beam Splitting

The theory of optimal beam splitting [14,15] consists of determining a continuous phase-only function

$$f(x) = \exp[i\varphi(x)] \tag{1}$$

that generates a set of diffraction orders with maximum overall efficiency η (defined as the sum of the normalized intensity of each target order). The notation in [14] is followed in this work. Let us consider a one-dimensional grating with a period of 2π. Then,

$$a_k = \frac{1}{2\pi}\int_{-\pi}^{\pi} \exp[i\varphi(x)]\exp[-ikx]\mathrm{d}x \tag{2}$$

is the kth Fourier coefficient of $f(x)$ in Eq. (1), and x is the spatial coordinate. The phase-only function for optimal beam splitting is calculated as

$$\exp[i\varphi(x)] = \frac{s(x)}{|s(x)|}, \tag{3}$$

where

$$s(x) = \sum_k \mu_k \exp[i\alpha_k]\exp[ikx], \tag{4}$$

where k is the integer index of each of the N target orders, and α_k and μ_k, are the sets of numerical parameters, which represent the phase and amplitude of each harmonic component, respectively.

The phases α_k of each target order are the variables to be first computationally determined in order to achieve the highest η possible. Afterward, the amplitudes μ_k are included in the optimization to distribute the energy among the target diffracted orders with a predetermined constraint on the Fourier coefficients a_k. The optimization of Eqs. (2)–(4) can be performed with advanced numerical tools. We used the SOLVER routine in Microsoft Excel, which employs a generalized reduced gradient algorithm [28]. The result is a phase-only mapping that can be applied to transform a linear phase blazed grating profile $\exp(i2\pi x/p)$ onto the optimal phase profile $\varphi(x)$). Here, p denotes the period of the grating. The same type of phase mapping can be then applied to produce generalized optimal gratings, as shown later.

The theory detailed in [14,15], was recently experimentally demonstrated in [19] using phase-only SLMs, to produce equi-intense orders. The generation of orders with tailored intensity was also demonstrated in [20]. The experimental realization of this theory has been always applied to obtain light spots at symmetric positions. Here, on the contrary, we first extend the optimization routine to generate grating profiles where different orders can be selectively eliminated or enhanced, producing an asymmetric pattern of diffracted orders.

In addition, we also show how the phase of the various orders can be tailored as well. The result allows complete optimization of a desired grating structure to control the number, intensity, and phase of various diffracted orders. Moreover, the grating phase profile can be applied to a variety of different DOE problems as demonstrated here. Experimental results agree very well with theory, as shown next.

3. Experiments and Discussion

Experiments were carried out with two systems. In one system [19], we used a reflective LCoS-SLM for visible wavelengths (400–700 nm), model X10468-01 from Hamamatsu. A 514 nm wavelength beam from a tunable Ar ion laser is spatially filtered and expanded to illuminate the SLM. A physical positive lens is used to focus the output beams onto a CCD camera (Basler scA1390-17fc). For the second system [20], we used a transmissive parallel-aligned Epson LCD, also with a 514 nm laser wavelength as detailed previously. Both devices produce a phase modulation range exceeding 2π rad for the selected wavelength.

A. Asymmetric Output Beam Splitter Gratings

Asymmetric beam splitting is demonstrated with several examples of equi-intense focused beams where we generate a series of gratings having different asymmetric sets of diffracted orders. Figure 1 shows images of experimental results, captured with the CCD camera. Each grating has a different phase profile generated after the proper look-up table is applied to the blazed grating following the optimization of the parameters in Eqs. (3) and (4). Two periods of each encoded phase profile are also shown in the figure. The original blazed phase profile is also shown at the top of the figure. The gratings were all designed with a period of 32 pixels. Rows D1–D5 show different cases for optimal duplicators ($N = 2$). Row D1 corresponds to the π-phase binary grating, which was identified as the optimal symmetric duplicator in [16]. Two strong $\pm$1st orders take most of the energy ($\eta = 8/\pi^2$) although other weak undesired orders are also visible at odd orders. These other beams

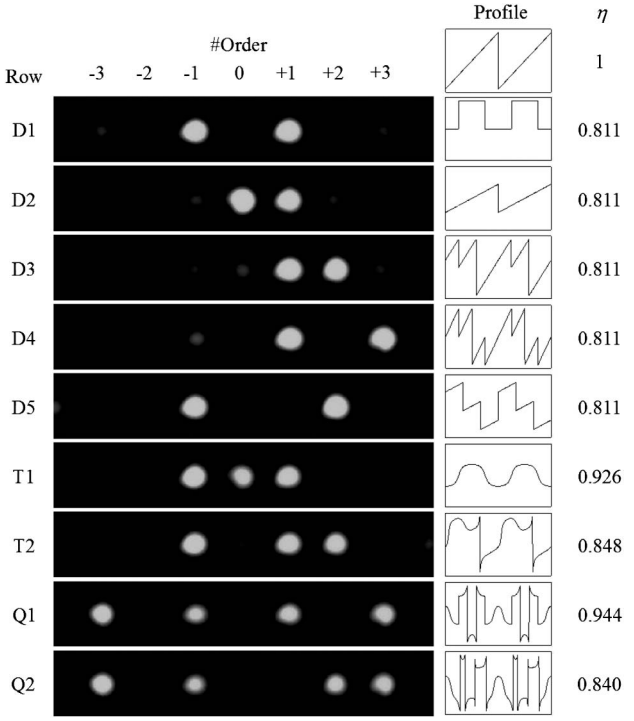

Fig. 1. Experimental asymmetric beam splitting for duplicators ($N = 2$, rows D1–D5), triplicators ($N = 3$, rows T1 and T2) and quadruplicators ($N = 4$, rows Q1 and Q2). Two periods of the encoded phase profile to obtain each result are included (vertical axis is phase from −3.5 to 3.5 rad and horizontal axis is the spatial coordinate in arbitrary units). Overall theoretical efficiencies (η) are added as well.

appear similarly in all other duplicators but in different diffracted orders. Images have been saturated to clearly visualize the intensity difference between desired and undesired orders. Note in Fig. 1, row D2, that the optimal duplicator with target orders 0th and +1st is a blazed grating with a phase modulation of π rad (instead of the 2π of a usual blazed grating). This is therefore a particular case of the gratings proposed in [21]. The other duplicators in Fig. 1 are obtained with different variations of the blazed grating phase profile. Duplicators D3 and D4 are asymmetric, also with both orders positive (+1st and +2nd, and +1st and +3rd, respectively). Differently, duplicator D5 is asymmetric with target orders +2nd and −1st. Efficiencies in all these cases are practically the same as for the binary π-phase grating, $\eta = 8/\pi^2 = 0.811$ [16].

For triplicators ($N = 3$), the efficiency is greatly enhanced, with values over 0.9. Row T1 in Fig. 1 shows the optimal triplicator proposed by Gori *et al.* [16], derived as $\tan[\varphi(x)] = 2\mu \cos(x)$ with $\mu = 1.32859$ and $\eta = 0.926$. In row T2, we demonstrate an asymmetric triplicator by sending light to the ±1st and +2nd orders. This last case shows a slight reduction of the overall efficiency to $\eta = 0.848$. We apply a similar treatment for quadruplicators ($N = 4$), as shown in rows Q1 and Q2, where an equidistant and an asymmetric beam splitter are set, respectively. Although the calculated efficiency varies from $\eta = 0.944$ when it is symmetric to $\eta = 0.840$ when it is asymmetric, it can be still considered very efficient.

Some considerations must be taken in the experimental result with respect to theoretical values. Because the SLMs are pixelated devices, the designed continuous phase profile is not exactly reproduced. The output depends on the number of pixels that reproduce each phase period, and whether the period transition points correspond exactly to the pixel locations. These effects depend on the selection of the grating period. However, the diffraction orders are produced by a Fourier transform operation, which is a global integral across the entire grating. Therefore, errors in one region might be offset by the opposite errors in other regions, depending on the selected grating period.

Note that we are creating a Fourier series from the periodic transmission function. When we encode this, we create different harmonics in the original transmission function. Consequently, we would expect to see additional diffracted orders, but no scattering from the sharp transition points. One example that supports this idea is a perfectly blazed grating. The phase abruptly goes from 2π to 0 at the transition point. However, this does not cause any scattering.

We have experimentally tested different grating periods and the selected value of 32 pixels has been verified to produce good results. Table 1 gives numerical values of the relative intensities of the diffraction orders generated in each case. Values have been normalized to the maximum value in each case. These data show a very good reproduction of the target diffraction orders, although some variation in the intensity values happens, especially for the quadruplicators. These gratings require rapid changes in the phase profile, which are more difficult to reproduce with the SLM. This problem will become less important with microfabricated devices or with higher resolution devices.

In spite of these effects, the results in Fig. 1 demonstrate the extreme flexibility of this approach to

Table 1. Numerical Values of the Intensity of the Diffraction Orders for the Different Cases in Fig. 1. Values are Normalized to the Maximum Value in Each Case. Values for the Target Orders are Indicated with Bold Font

	Order						
Plot	−3	−2	−1	0	1	2	3
D1	0.13	0.00	**1.00**	0.01	**1.00**	0.00	0.11
D2	0.00	0.03	0.11	**1.00**	**0.89**	0.10	0.01
D3	0.00	0.00	0.10	0.17	**0.98**	**1.00**	0.11
D4	0.01	0.00	0.21	0.00	**0.97**	0.00	**1.00**
D5	0.02	0.02	**0.93**	0.02	0.02	**1.00**	0.02
T1	0.01	0.04	**1.00**	**0.84**	**0.91**	0.13	0.01
T2	0.00	0.01	**1.00**	0.10	**0.94**	**0.93**	0.01
Q1	**1.00**	0.00	**0.75**	0.01	**0.87**	0.07	**0.93**
Q2	**1.00**	0.01	**0.71**	0.02	0.01	**0.84**	**0.88**

generate sets of phase profiles for desired gratings. Note that the new phase profiles for each case shown in the figure, provide the data for the phase-transformation look-up table that can be applied to other arbitrary phase optical elements.

B. Phase Control

The method in [14,15] can also be applied to control the relative phases of these diffracted orders. Note that a_k, defined in Eq. (2), is a complex value, which can be written as a modulus-argument product as

$$a_k = |a_k| \exp(i\beta_k), \tag{5}$$

where β_k denotes the argument of the kth diffraction order. Usually, the constraint employed to resolve the variables α_k and μ_k has always been imposed to the modulus $|a_k|$. Here, we also impose a constraint to the value of β_k.

For instance, let us consider $N = 3$ with 0th and ± 1st as target orders with equal intensity. For simplicity, we set no phase difference between -1st and $+1$st orders but we change their phase relation with respect to the 0th order. Three-beam interference is captured at the output to demonstrate phase control. This is obtained by displaying a low frequency grating and placing the CCD in a plane close to the display, so that the three beams overlap. Figure 2(a) shows the expected intensity profiles of the interference of these three beams, when the phase difference between 0th and ± 1st orders is $0, \pi/2$, and π rad. The typical three-beam interference (with two zeros and a weak maximum in between two intense maxima) is produced when the phase difference is 0 or π, giving both the same result but with a spatial shift. However, when the phase difference is $\pi/2$, a sinusoidal variation with reduced contrast is obtained. Figure 2(b) shows the captured experimental images of all three simulated cases. As seen in the figure, these interference patterns match calculations.

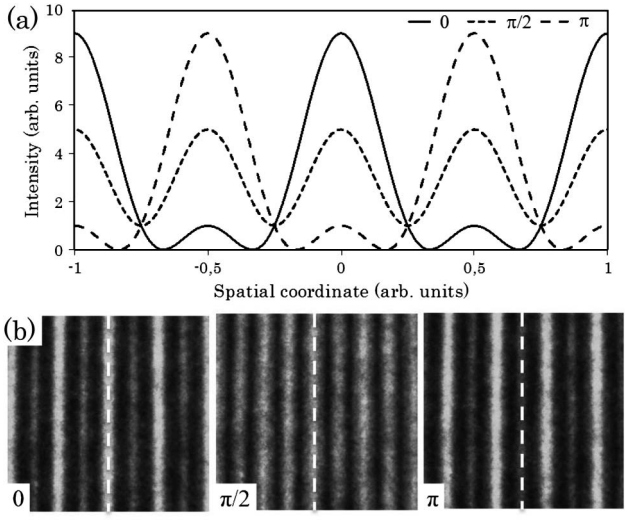

Fig. 2. Three beam interference of 0th and ± 1st diffracted orders, produced to demonstrate control of the relative phase among orders: (a) simulated intensity profiles when the phase difference between 0th and ± 1st is $0, \pi/2$, and π and (b) captured intensities of all three cases. Dashed lines in (b) mark the same position.

4. Applications to Generalized Diffractive Elements

As we mentioned earlier, the grating beam splitting can be viewed as the result of a phase-only mapping that transforms a linear phase profile $\phi(x) = 2\pi x/p$ onto the optimal phase profile

$$\varphi(x) = \varphi[\phi(x)], \tag{6}$$

where p is again the period of the grating. Therefore, it is very relevant to note that the above derived grating profiles can be generalized to DOEs other than linear gratings. For that purpose, the phase look-up function $\varphi(\phi)$ is simply applied to an arbitrary phase function $\phi(x,y)$ as discussed in the introduction.

For instance, let us consider a converging lens phase profile, which is given by the phase function:

$$\exp[i\phi(r)] = \exp\left[\frac{i\pi r^2}{\lambda f}\right], \tag{7}$$

where r is the radial coordinate, λ is the wavelength and f is the focal length of the lens. If now we substitute the phase profile $\varphi(\phi)$ of Eq. (7) in (6), the beam splitter profile is applied onto a converging lens. Then, each n harmonic component will provide a focal length $f_n = f/n$ [6].

Let us assume now that we have generated the duplicator phase profile ($N = 2$) that generates the 1st and 2nd orders. When we apply this duplicator phase profile to the converging lens profile, it will produce a pure converging bifocal lens. The first harmonic component focuses at a distance f, while the second harmonic component focuses at distance $f/2$. Similar multifocusing lenses can be generated using each of the phase profiles shown in Fig. 1.

We can additionally introduce a defined relative phase difference between the two orders. Then, tailored interference is produced. As an example, Fig. 3 shows the grey-level-encoded phase profiles of two different lenses displayed on the SLM. We encode lenses with large enough focal length to avoid other effects caused by the spatial resolution limits of the display. First, the quadratic phase profile of a regular diffractive lens with a focal length f as the one defined in Eq. (7) is displayed in Fig. 3(a), together with the transverse cut of the phase values at one diameter. Figure 3(b) corresponds to the same lens when a phase look-up table is applied corresponding to the duplicator phase profile to obtain 1st and 2nd order. This new diffractive lens thus creates a bifocal lens that focuses at the original focal length (f), but also at a distance $f/2$. A schematic view of this realization is shown in Fig. 3(c). These two focusing beams have the same energy. Therefore, a plane can be found in between the two focalizations where both beams illuminate the same area, thus having equal intensity.

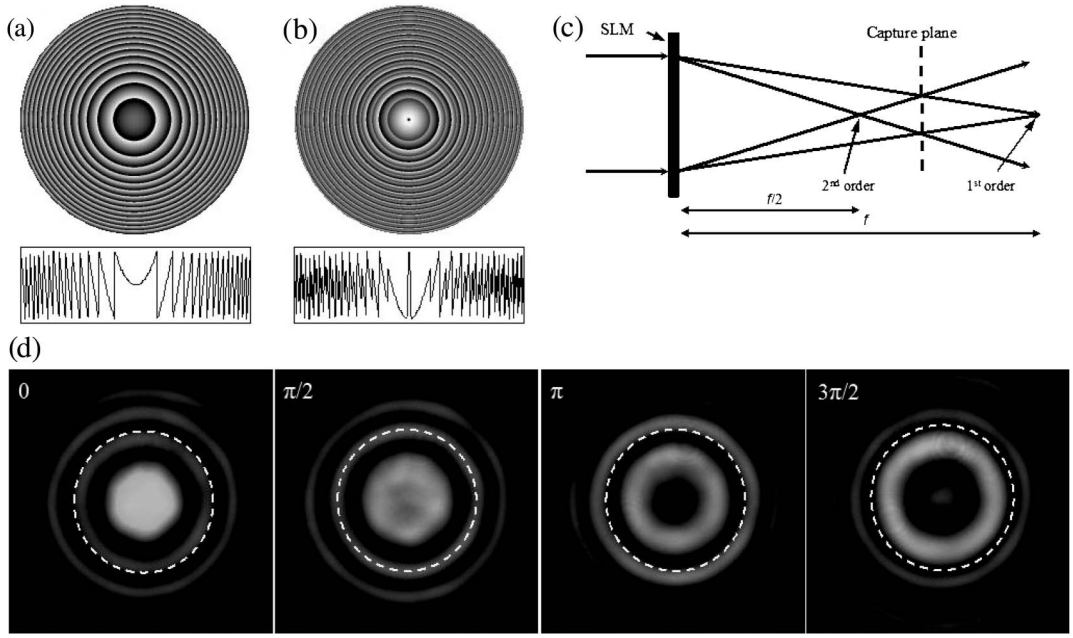

Fig. 3. Phase profiles of diffractive lenses: (a) a standard converging lens, (b) lens in Fig. 3(a) encoded as a duplicator with 1st and 2nd order, and with an argument difference of π. Both include a transverse phase profile from the center of the image (the vertical axis denotes phase values from –3.5 to 3.5 rad, and horizontal scale is the spatial coordinate in arbitrary units), (c) schematic view of the bifocal lens focalizations and the position of the capture plane where the CCD camera is placed, and (d) experimental interference pattern of the bifocal lens produced with the duplicator lenses. The phase difference between both orders changes in steps of $\pi/2$.

This is denoted as the capture plane in Fig. 3(c). Thus, the interference of these two beams will show interference rings with maximum contrast. By positioning the CCD camera at that plane, an interference pattern as the one in Fig. 3(d) can be captured. In each of the images, a different value is applied to the phase difference between 1st and 2nd order beams, by $\pi/2$ steps [the design presented in Fig. 3(b) corresponds to an argument difference between orders equal to π rad]. A ring with fixed size and position is superimposed in all four experimental images to notice the interference fringes displacement, which are all in agreement with the phase steps imposed between the two beams. This control of the diffracted orders phase, added to the control of their intensity shown previously in [20], greatly extends the field of application of the optimal beam splitting theory.

As a final example, let us now consider a spiral phase profile $\exp[i\ell\theta]$, where θ denotes the azimuthal angle and ℓ is an integer denoting the number of 2π ramps in the spiral phase mask. It is well known that the spiral phase generates a vortex beam with topological charge ℓ [29]. When focused, the vortex beam results in the typical doughnut pattern where the diameter of the doughnut focus pattern increases as the topological charge of the vortex beam increases. The combination of two vortex beams with equal topological charge but opposite sign $\pm\ell$, generates an intensity interference pattern between both doughnut beams as $\cos^2(2\ell\theta)$. The result is an annulus of light presenting 2ℓ nulls along the azimuthal angle. Note that if a spiral phase profile is simply binarized to obtain only two levels with π rad phase difference, the main contributions are the $\pm$1st harmonic components, and therefore the same interference of the beams will be produced [30].

If we extend the grating beam splitting in Eq. (6) to the spiral phase profile $\exp[i\ell\theta]$, we can achieve different situations for the harmonic components. As an example, let us set a quadruplicator pattern ($N = 4$) with target orders $\pm$1st and $\pm$3rd (as the one in Fig. 1, row Q1) applied to a spiral phase of $\ell = 3$. The $\pm$1st harmonic components will produce the interference of the vortex beams with charges $\ell = \pm 3$. The $\pm$3rd harmonic components will produce vortices with charges $3\ell = \pm 9$. Therefore, the combination should produce two dashed rings with different diameters.

However, several considerations must be taken into account for a proper result to be obtained. First, the original optimal quadruplicator sends the same amount of light into all diffracted orders. However, as the radius of the doughnut beams is different, the intensity of the outer ring would be lower than the inner one. Therefore, intensity compensation proportional to the radius must be applied for equalization as demonstrated previously in [20]. Second, and thanks to the phase control, the relative position of the constructive and destructive interference between both rings can be arbitrarily set. If a phase shift Φ is introduced between the two first-orders, then the intensity of the interference pattern will rotate as $\cos^2(2\ell\theta + \Phi)$. This feature is especially interesting for applications where light must be precisely aligned.

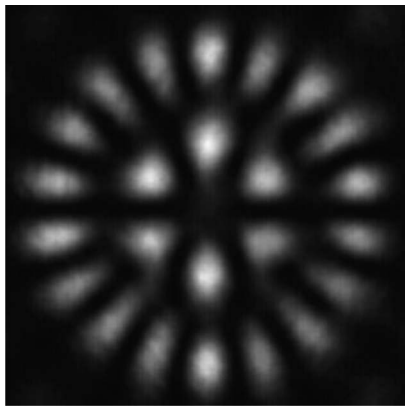

Fig. 4. Excerpt of the captured experimental output of the optimal beam splitter of $N = 4$ at $\pm$1st and $\pm$3rd orders, applied to a spiral phase profile. In the media file, a phase shift Φ is added in steps of $\pi/2$, first between the $\pm$1st (resulting in the rotation of the inner circle) and second between the $\pm$3rd orders (resulting in the rotation of the outer circle) (media 1).

Figure 4 shows the experimental result of this example. These last results have been obtained with the system employing the transmissive display [20]. In the image, the two interference patterns are clearly visible. The inner ring, corresponding to the $\pm$1st orders, shows the interference of the $\ell = \pm 3$ vortex beams, with six maxima and six minima along the angular direction. The outer ring, which corresponds to the $\pm$3rd orders, shows the interference of the $\ell = \pm 9$ vortex beams, with 18 maxima and 18 minima.

Now, a relative phase shift Φ can be introduced either onto the $\pm$1st orders, or onto the $\pm$3st orders that will rotate the corresponding interference pattern. In order to more clearly see the rotation in the interference patterns, a movie was captured where the different cases are reproduced sequentially. First, the phase shift Φ is introduced in steps of $\pi/2$ among the $\pm$1st orders, while keeping the relative phase between the $\pm$3rd orders constant. This rotates the interference pattern in the inner ring, while the interference in the outer ring is kept constant. Then, the phase shift Φ is introduced onto the third-order, again in steps of $\pi/2$, while the phase among $\pm$1 orders is kept constant. Note that a separate optimization procedure is required for each phase step change. Following this sequence, the resulting interference pattern shown in the movie first rotates in the inner ring, and then the interference pattern from the outer ring changes position at the same rate. The relative phase difference between doughnut beams generated at $\pm$1st and $\pm$3rd orders is visible in each case in the rotation of the interference pattern of the inner with respect to the outer ring.

5. Conclusions

In conclusion, we have demonstrated the potential of the phase-only beam splitting theory developed by Romero and Dickey [14,15] to design DOEs with novel and interesting features. Here we have shown experimental results that extend the approach in two ways. First, we have applied it to the design of gratings with asymmetric diffraction patterns. We have also demonstrated the control of the relative phase between the different diffracted orders. Finally we show that the phase profiles generated by this approach can be generally applied to other DOEs, such as diffractive lenses or spiral phase masks for the generation of optical vortices, where the potential of the optimal method is exploited for controlling the intensity, asymmetry, and phase of these DOEs. In spite of the resolution limits imposed by the use of pixelated devices, experimental results that validate the designs have been reported using phase-only SLMs. Using higher pixelated devices and slightly different periods, these results could be improved. However, the basic result shows the ability to obtain a variety of nonsymmetric grating outputs.

As discussed in the introduction, similar results could be obtained by using iterative approaches. However, the advantage of this approach is that we begin with a blazed profile for the optical element. We then simply apply a phase transformation look-up table that easily produces the desired set of output beams to the blazed version of other DOEs.

IM acknowledge financial support from Ministerio de Enonomía y Competitividad from Spain (ref. FIS2012-39158-C02-02). JA acknowledges the financial support from the Ministerio de Educación of Spain through the Programa Nacional de Movilidad de Recursos Humanos del Plan Nacional de I+D+i 2008-2011.

References

1. L. P. Lesem, P. M. Hirsch, and J. A. Jordan, "The kinoform: a new wavefront reconstruction device," IBM J. Res. Dev. **13**, 150–155 (1969).
2. D. C. O'Shea, J. W. Beletic, and M. Poutus, "Binary-mask generation for diffractive optical elements using microcomputers," Appl. Opt. **32**, 2566–2572 (1993).
3. H. Dammann and K. Görtler, "High-efficiency in-line multiple imaging by means of multiple phase holograms," Opt. Commun. **3**, 312–315 (1971).
4. C. Zhou and L. Liu, "Numerical study of Dammann array illuminators," Appl. Opt. **34**, 5961–5969 (1995).
5. G. Saavedra, W. D. Furlan, and J. A. Monsoriu, "Fractal zone plates," Opt. Lett. **28**, 971–973 (2003).
6. V. Moreno, J. F. Román, and J. R. Salgueiro, "High efficiency diffractive lenses: deduction of kinoform profile," Am. J. Phys. **65**, 556–562 (1997).
7. I. Moreno, J. A. Davis, D. M. Cottrell, N. Zhang, and X. C. Yuan, "Encoding generalized phase functions on Dammann gratings," Opt. Lett. **35**, 1536–1538 (2010).
8. J. L. Horner and J. R. Leger, "Pattern recognition with binary phase-only filters," Appl. Opt. **24**, 609–611 (1985).
9. R. W. Gerchberg and W. O. Saxton, "A practical algorithm for the determination of phase from image and diffraction plane pictures," Optik **35**, 237–246 (1972).
10. J. Bengtsson, "Design of fan-out kinoforms in the entire scalar diffraction regime with an optimal-rotation-angle method," Appl. Opt. **36**, 8435–8444 (1997).
11. R. Di Leonardo, F. Ianni, and G. Ruocco, "Computer generation of optimal holograms for optical trap arrays," Opt. Express **15**, 1913–1922 (2007).

12. D. Prongué, H. P. Herzig, R. Dändliker, and M. T. Gale, "Optimized kinoform structures for highly efficient fan-out elements," Appl. Opt. **31**, 5706–5711 (1992).
13. J. N. Mait, "Design of binary-phase and multiphase Fourier gratings for array generation," J. Opt. Soc. Am. A **7**, 1514–1518 (1990).
14. L. A. Romero and F. M. Dickey, "Theory of optimal beam splitting by phase gratings. I. One-dimensional gratings," J. Opt. Soc. Am. A **24**, 2280–2295 (2007).
15. L. A. Romero and F. M. Dickey, "The mathematical theory of laser beam-splitting gratings," Prog. Opt. **54**, 319–386 (2010).
16. F. Gori, M. Santarsiero, S. Vicalvi, R. Borghi, G. Cincotti, E. Di Fabrizio, and M. Gentili, "Analytical derivation of the optimum triplicator," Opt. Commun. **157**, 13–16 (1998).
17. V. Y. Miklyaev, W. Imgrunt, T. Bizjak, L. Aschke, V. N. Lissotschenko, V. S. Pavelyev, and D. G. Kachalov, "Novel continuously shaped diffractive optical elements enable high efficiency beam shaping," Proc. SPIE **7640**, 764024 (2010).
18. Yu. V. Miklyaev, A. Krasnaberski, M. Ivanenko, A. Mikhailov, W. Imgrunt, L. Aschke, and V. N. Lissotchenko, "Efficient diffractive optical elements from glass with continuous profiles," Proc. SPIE **7913**, 79130B (2011).
19. J. Albero and I. Moreno, "Grating beam splitting with liquid crystal adaptive optics," J. Opt. **14**, 075704 (2012).
20. J. Albero, I. Moreno, J. A. Davis, D. M. Cottrell, and D. Sand, "Generalized phase diffraction gratings with tailored intensity," Opt. Lett. **37**, 4227–4229 (2012).
21. J. A. Davis, D. M. Cottrell, J. Campos, M. J. Yzuel, and I. Moreno, "Encoding amplitude information onto phase-only filters," Appl. Opt. **38**, 5004–5013 (1999).
22. J. Ren and P. Guo, "Study on four-step computer-generated hologram with same diffraction efficiency of the zeroth and first-order," Opt. Eng. **50**, 08501 (2011).
23. J. A. Davis, J. Adachi, C. R. Fernández-Pousa, and I. Moreno, "Polarization beam splitters using polarization diffraction gratings," Opt. Lett. **26**, 587–589 (2001).
24. C. R. Fernández-Pousa, I. Moreno, J. A. Davis, and J. Adachi, "Polarization diffraction-grating triplicators," Opt. Lett. **26**, 1651–1653 (2001).
25. A. Jesacher and M. J. Booth, "Parallel direct laser writing in three dimensions with spatially dependent aberration correction," Opt. Express **18**, 21090–21099 (2010).
26. J. B. Bentley, J. A. Davis, M. A. Bandres, and J. C. Gutiérrez-Vega, "Generation of helical Ince–Gaussian beams with a liquid–crystal display," Opt. Lett. **31**, 649–651 (2006).
27. J. B. Bentley, J. A. Davis, J. Albero, and I. Moreno, "Self-interferometric technique for visualization of phase patterns encoded onto a liquid-crystal display," Appl. Opt. **45**, 7791–7794 (2006).
28. http://support.microsoft.com/kb/214115.
29. M. W. Beijersbergen, R. P. C. Coerwinkel, M. Kristensen, and J. P. Woerdman, "Helical-wavefront laser beams produced with a spiral phaseplate," Opt. Commun. **112**, 321–327 (1994).
30. J. A. Davis, E. Carcole, and D. M. Cottrell, "Nondiffracting interference patterns generated with programmable spatial light modulators," Appl. Opt. **35**, 599–602 (1996).